Quantum Electronics **33** (1) 69 – 75 (2003)

NONLINEAR-OPTICAL PHENOMENA

PACS numbers: 42.65.Jx; 42.65.Ky; 52.50.Jm
DOI: 10.1070/QE2003v033n01ABEH002366

Nonlinear-optical transformation of a high-power femtosecond laser pulse in air

V.P. Kandidov, O.G. Kosareva, A.A. Koltun

***Abstract*. A change in the spectrum and the energy distribution of the light field of a high-power femtosecond laser pulse is studied numerically in a broad range of its spatial scales. It is shown that the effect of filamentation, the generation of a supercontinuum and conical emission, the formation of a ring structure in the distribution of the pulse energy and other effects observed during the propagation of the laser pulse in air are caused by the nonlinear-optical transformation of the light field in the region with dimensions exceeding substantially the transverse size of the filament. The pulse filamentation is accompanied by the redistribution of power in its cross section. The spatio – temporal characteristics of emission calculated for femtosecond laser systems are in quantitative agreement with the experimental data.**

Keywords: *femtosecond nonlinear optics, filamentation, supercontinuum.*

1. Introduction

The self-action of ultrashort laser pulses propagating in gases has long attracted attention of researchers (see, for example, [1 – 4]). For pulses with peak intensities of $10^{13} - 10^{14}$ W cm^{-2} focused into cells filled with inert gases at high pressures, the broadening of the frequency spectrum and the formation of ring structures in the spatial distribution of the fluence were observed [1 – 3]. It has been found that the change in the spectrum and the spatio – temporal profile of the pulse is caused by nonlinear defocusing in a plasma caused by the multiphonon ionisation of gas atoms in a strong light field of the focused beam [4].

The effect of filamentation of femtosecond laser pulses in air at the atmospheric pressure was discovered in the mid-1990s [5 – 7]. The filamentation was observed for 150 – 230-fs, 0.8-μm pulses with peak power of 5 – 50 GW. The effect of filamentation is manifested in the localisation of a significant fraction of the energy of a collimated pulse within a narrow axial region over a length of a few tens – hundreds metres, which is accompanied by the generation of a supercontinuum, whose branch lying in the visible range is located within a narrow cone encompassing the filament [8]. The supercontinuum band generated by terawatt 35-fs pulses extends from 0.5 to 4.5 μm [9]. Recently, the possibility of using a broadband supercontinuum for a broadband laser probing of the atmosphere was discussed [10]. In the first experiments with a femtosecond lidar [11] the absorption spectra of oxygen and water vapour were obtained, which coincide with the spectra calculated using the HITRAN data base.

From the point of view of nonlinear optics, the filamentation is caused by the nonstationary self-action of a femtosecond laser pulse whose peak power exceeds the critical power of self-focusing in air. Filamentation appears due to the Kerr nonlinearity of neutral atoms and molecules in air, as well as due to the nonlinearity of the laser plasma produced upon photoionisation in a strong light field. The model of moving foci [12], modified taking into account the nonlinear diffraction of radiation in the laser plasma [13], allows one to explain filamentation observed in experiments. The temporal slices of the pulse are focused into a continuous sequence of points, by forming the filament. As the radiation intensity in a nonlinear focus increases, the probability of multiphoton ionisation also increases, and a laser plasma is produced, which causes the aberration defocusing of subsequent pulse slices. For this reason, upon filamentation of a laser pulse in air, the moving foci exist only for the leading edge of the pulse, whereas at the pulse tail a complicated ring structure of the radiation intensity distribution is formed.

The theoretical studies of filamentation are based on a nonlinear-optical wave model of propagation of a powerful femtosecond laser pulse in air. The model describes the nonstationary nonlinearity caused by the cubic susceptibility of gaseous components in the air and laser plasma. This model was analysed using the variation approach [14] and paraxial approximation [15] – the methods that are well known in the theory of self-action of laser beams (see, for example, [16, 17]). The nonstationary multidimensional problem of filamentation can be studied in detail only by numerical methods. At present, the physical picture of formation of filaments [18-20], refocusing effect [13], generation of a conical supercontinuum emission [8, 21], and the appearance of random displacements of filaments [22, 23] has been obtained using numerical simulations. However, the known numerical solutions do not reproduce completely

V.P. Kandidov, A.A. Koltun Department of Physics, M.V. Lomonosov Moscow State University, Vorob'evy gory, 119992 Moscow, Russia; e-mail: kandidov@msuilc.ilc.msu.su;
O.G. Kosareva. International Teaching and Research Laser Center, M.V. Lomonosov Moscow State University, Vorob'evy gory, 119992 Moscow, Russia; e-mail: kosareva@msuilc.ilc.msu.su

Received 18 June 2002
Kvantovaya Elektronika **33** (1) 69 – 75 (2003)
Translated by M.N. Sapozhnikov

the spatio–temporal deformation of the light field produced by a pulse propagating from the output aperture of a laser system to the site where a filament is formed. Because the spatial scale of the light field is limited, it is usually assumed in the numerical model that the output laser pulse has a diameter that is close to that of the filament, and the peak intensity of this pulse is close to that of the filament.

In this paper, we study changes in the spectrum and distribution of the light-field energy during the propagation of a powerful pulse in air, whose parameters correspond to the output parameters of femtosecond lasers used in filamentation experiments. The main attention is devoted to the adequate description of the pulse transformation both in the filament region and over its entire cross section. The problem is simulated numerically by the original method, which allows us to reproduce a broad range of spatial scales in the beam cross section.

2. Analysis of the available experimental and theoretical results

By considering the known experimental data on the filamentation of powerful femtosecond pulses in air, we discuss the effects for which the results of theoretical studies do not agree quantitatively with the experimental data. One of these effects is the so-called stabilisation of the filament parameters. According to estimates [6, 24], the light-field intensity in a filament is close to $I_f = 5 \times 10^{13}$ W cm^{-2} – the intensity at which the electron concentration in the induced laser plasma is such that defocusing in the plasma restricts an increase in the pulse intensity caused by the Kerr self-focusing. The diameter of a filament being formed is ~ 100 μm, irrespective of the pulse power, and its energy amounts to 10 %–12 % of the total pulse energy [5–7]. The numerical simulations failed to predict the stabilisation of the produced filament, which was observed in experiments.

The measurements of the fluence in the cross section of the pulse revealed a system of concentric rings with a centre on the filament axis. Their number achieves five–six in the case of a collimated output beam of a femtosecond laser (Fig. 1a) [25]. When the beam is focused, more than ten narrow, closely spaced energy-density rings are formed [26]. However, numerical simulations could give only one ring near the filament axis [19, 21].

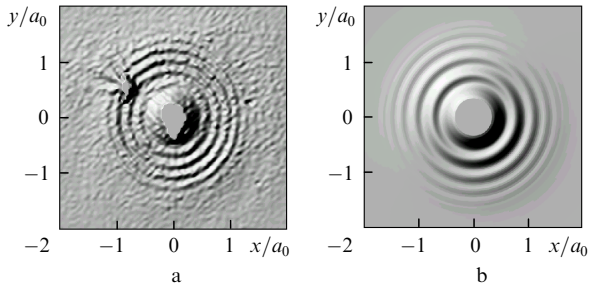

Figure 1. Distributions of the fluence in the pulse cross section upon filamentation of a collimated laser beam in air. The distributions are obtained (a) in the laboratory experiment (the 1/e pulse duration $\tau_0 = 54$ fs, the pulse energy $W = 14$ mJ, the beam radius $a_0 = 7.5$ mm, the distance $z = 86$ m [25]) and (b) in the numerical experiment ($\tau_0 = 280$ fs, $W = 10$ mJ, $a_0 = 3.5$ mm, $z = 35$ m).

The generation of a supercontinuum was studied by using the most comprehensive models on the nonstationary nonlinear-optical interaction of powerful radiation with air [21]. These models take into account the instant and delayed components of the cubic susceptibility of neutral atoms and molecules, the higher-order material dispersion, and the process of plasma generation, described by the Perelomov–Popov–Terent'ev theory of photoionisation [27], in which the effective charge of singly ionised oxygen molecules measured in experiments is used [28]. In papers [29, 30], the next terms of the expansion on the method of slowly varying amplitudes are also taken into account, which allows one to describe an increase in the steepness of the pulse leading edge in the case of strong nonlinearity. At the same time, the width of the visible supercontinuum band, obtained numerically using the overestimated self-steepening parameter of the pulse, proved to be lower than the experimental width (Fig. 2). According to the experimental data [8], the divergence angle for supercontinuum emission increases with the frequency shift to the blue, achieving 0.12° at a wavelength of 0.5 μm. At present, only the relative divergence angle of conical supercontinuum emission in the 0.75–0.67-μm range was determined numerically (see insert in Fig. 3) [21].

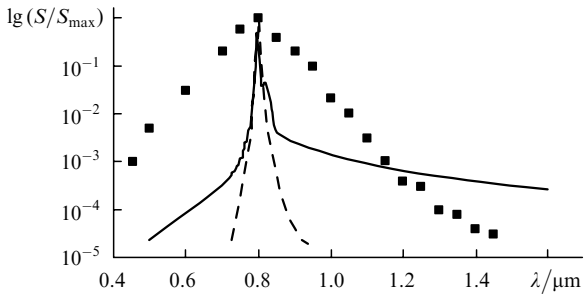

Figure 2. Dependences of the normalised spectral intensity S/S_{max} of a pulse on the wavelength λ obtained experimentally (points) for $\tau_0 = 35$ fs, $a_0 = 25$ mm (at the 0.5 level), and the peak power $P_{max} = 2$ TW [9], and by numerical simulation for a 140-fs pulse with initial parameters that are close to those of the filament ($a_0 = 170$ μm, the initial peak intensity $I_0 \approx 10^{13}$ W cm^{-2} (dashed curve) [21] and coincide with real parameters of the laser output beam ($a_0 = 3.5$ mm, $I_0 \approx 10^{11}$ W cm^{-2}) (solid curve).

The quantitative difference between theoretical and experimental results appears due to the errors in calculations of the light field in a broad peripheral region embracing a narrow filament. The numerical model, in which a pulse with parameters close to those of the filament is considered, cannot reproduce accurately the energy exchange between the intense light field on the beam axis and a low-intensity background field at the beam periphery. A qualitative analysis shows that the redistribution of the light energy in the beam cross section plays a key role in filamentation. The localisation of energy in a narrow spatial region near the beam axis, refocusing, and formation of ring structures in the beam cross section, generation of a supercontinuum, whose short-wavelength part represents conical emission, occur due to the nonlinear-optical transformation of the light field over the entire cross section of the beam emitted by a femtosecond laser.

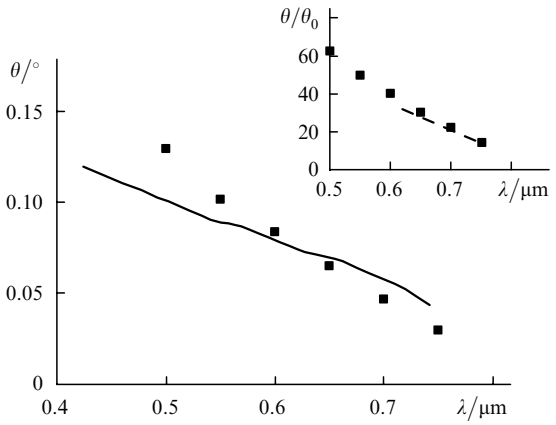

Figure 3. Dependences of the wavelength λ on the divergence angle θ in the visible band of a supercontinuum upon filamentation of a pulse with $\tau_0 = 140$ fs, $a_0 = 3.5$ mm, and $P_{\max} = 38$ GW, which were obtained experimentally [8] (squares) and by numerical simulations (solid curve). The insert shows the experimental dependence [21] (squares) and numerical simulation for radiation with initial parameters close to those of the filament ($a_0 = 170$ μm, $I_0 \approx 10^{13}$ W cm^{-2}) (dashed curve); θ_0 is the diffraction divergence angle.

3. Nonlinear-optical model

The cubic susceptibility of the gaseous components of air is determined by the anharmonicity of the electronic response and stimulated Raman scattering at the rotational transitions of neutral molecules. The characteristic time of the establishment of the electronic response is $\sim 10^{-15}$ s and it can be assumed instantaneous for femtosecond pulses, whereas Raman scattering is an inertial process [31, 32]. Assuming that the contributions from these mechanisms are identical for a long pulse [32], the nonlinear increment $\Delta n_{\rm K}(r,z,t)$ of the refractive index of air in the light field with the amplitude $E(r,z,t)$ can be written in the form

$$\Delta n_{\rm K}(r,z,t) = \frac{1}{2}\, n_2 \left[|E(r,z,t)|^2 + \int_{-\infty}^{t} H(t-t')|E(r,z,t')|^2 {\rm d}t' \right], \qquad (1)$$

where n_2 is the nonlinearity coefficient that was established for a long pulse, which is usually assumed equal to $(1.5-5.6)\times 10^{-19}$ cm^2 W^{-1} [32, 33]. The response function $H(t)$ of Raman scattering can be approximated by the expression [19]

$$H(t) = \Theta(t)\Omega^2 \exp\left(-\frac{\Gamma t}{2}\right)\frac{\sin(\Lambda t)}{\Lambda}, \qquad (2)$$

$$\Lambda = \left(\Omega^2 - \frac{\Gamma^2}{4}\right)^{1/2},$$

where $\Theta(t)$ is the Heaviside function. The characteristic delay times of the nonlinear response $\tau_1 = 2/\Gamma = 77$ fs and $\tau_2 = 1/\Lambda = 63$ fs are comparable with duration of pulses that are commonly used in filamentation experiments.

The peak intensity of a beam increases upon its self-focusing, and a laser plasma is produced when the photoionisation threshold is achieved. In the approximation of a single ionisation of neutral molecules, the concentration $N_{\rm e}(r,z,t)$ of free electrons is described by the equation

$$\frac{\partial N_{\rm e}(r,z,t)}{\partial t} = R(E(r,z,t))[N_0 - N_{\rm e}(r,z,t)], \qquad (3)$$

where N_0 is the concentration of neutral molecules and $R(E(r,z,t))$ is the rate of their ionisation. Because the ionisation potential of an oxygen molecule is lower than that of nitrogen, estimates show that atmospheric oxygen makes the dominant contribution to the generation of free electrons. The rate of single ionisation of an oxygen molecule is adequately described by the Perelomov–Popov–Terent'ev model for a hydrogen-like atom in the field of a plane polarised wave [27]

$$R(E(r,z,t)) = |C_{n^*l^*}|^2 f_{lm} E_{\rm i}\left(\frac{6}{\pi}\right)^{1/2}\left[\frac{2(2E_{\rm i})^{3/2}}{E(r,z,t)}\right]^{2n^*-|m|-3/2} \times (1+\gamma^2)^{|m|/2+3/4} A_m(\omega,\gamma)\exp\left[-\frac{2(2E_{\rm i})^{3/2}}{E(r,z,t)}\, g(\gamma)\right], \qquad (4)$$

where $\gamma = \omega(2E_{\rm i})^{1/2}/E(r,z,t)$ is the adiabatic Keldysh parameter; $E_{\rm i}$ is the ionisation potential of an atom; $n^* = Z(2E_{\rm i})^{-1/2}$ and $l^* \approx n^* - 1$ are the effective principal and orbital quantum numbers; and Z is the effective charge of the atomic core; l is the orbital quantum number; m is the projection of l on the electric-field direction. The coefficients $C_{n^*l^*}$ and f_{lm}, as well as the functions $A_m(\omega,\gamma)$ and $g(\gamma)$ are rather cumbersome and, hence, are not presented here. The expressions for them can be found in paper [28]. The effective charge Z of a singly ionised oxygen molecule is assumed equal to 0.75, according to experimental data [28].

The nonlinear increment in the refractive index caused by the laser plasma is

$$\Delta n_{\rm p}(r,z,t) = -\frac{\omega_{\rm p}^2(r,z,t)}{2n_0(\omega^2+\nu_{\rm c}^2)}\left(1 - {\rm i}\,\frac{\nu_{\rm c}}{\omega}\right), \qquad (5)$$

where $\omega_{\rm p}(r,z,t) = [4\pi e^2 N_{\rm e}(r,z,t)/m]^{1/2}$ is the plasma frequency and $\nu_{\rm c} \approx 6\times 10^{12}$ s^{-1} [34] is the effective frequency of collisions of electrons with molecules of the air components. Because the fundamental radiation frequency of a Ti : sapphire laser is $\omega = 2.35\times 10^{15}$ s^{-1}, then the inequality $\nu_{\rm c} \ll \omega$ is fulfilled during filamentation in air. In this case, expression (5) can be written in the form

$$\Delta n_{\rm p}(r,z,t) = -\frac{\omega_{\rm p}^2(r,z,t)}{2n_0\omega^2}. \qquad (6)$$

A change in the light field $E(r,z,t)$ in the approximation of slowly varying amplitudes is described by the expression

$$2{\rm i}k\left(\frac{\partial}{\partial z} + \frac{1}{v_{\rm gr}}\frac{\partial}{\partial t}\right)E(r,z,t) = \Delta_\perp E(r,z,t) + \frac{2k_0^2}{n_0} \times [\Delta n_{\rm K}(r,z,t) + \Delta n_{\rm p}(r,z,t)]E(r,z,t) - {\rm i}k_0\alpha(r,z,t)E(r,z,t), \qquad (7)$$

where $v_{\rm gr}$ is the group velocity; k_0 is the wave number;

$$\alpha = I^{-1} p\hbar\omega\left[\frac{\partial N_{\rm e}(r,z,t)}{\partial t}\right] \qquad (8)$$

is the absorption coefficient, which is determined by ionisation losses; $I = (cn_0/8\pi)|E^2|$ is the light-field intensity; and $p = 8$ is the order of a multiphoton process for the oxygen molecule.

Equation (7) neglects the group-velocity dispersion and an increase in the steepness of the pulse leading edge because here we consider the dependence of filamentation on spatial effects related to a change in the light field in the pulse cross section.

The pulse shape and the distribution of the fluence over its cross section, measured at the output of a femtosecond laser system, are close to Gaussians [6, 7]. Therefore, the complex component of the light field at $z = 0$ can be written in the form

$$E(r, z = 0, t) = E_0 \exp\left(-\frac{r^2}{2a_0^2} - \frac{t^2}{2\tau_0^2} + \mathrm{i}\,\frac{k_0 r^2}{2f}\right), \qquad (9)$$

where τ_0 and a_0 are the pulse duration and the beam radius; and f is the quantity that is inversely proportional to the initial curvature of the pulse front.

4. The investigation technique

The light field of a pulse (9) in a medium with homogeneous optical parameters has an axial symmetry, and the problem of finding $E(r, z, t)$ is three-dimensional (2D + t). The numerical solution of this problem with parameters corresponding to experimental parameters involves great difficulties. This is caused by a strong increase in the spatial and temporal scales of the light field upon filamentation. In experiments, pulses with the initial peak intensity $I_0 \approx 10^{11}$ W cm^{-2} and the output-beam radius $a_0 = 0.3 - 3$ cm are used. Upon filamentation, a fine structure is developed in the radial distributions of the intensity and phase of the field, which reflects the spatial localisation of energy and formation of rings in the beam cross section. The filament intensity exceeds the initial peak intensity value more than by two orders of magnitude. The filament diameter is of about 100 μm, irrespective of the output laser beam diameter. The width of the frequency spectrum of the pulse increases few orders of magnitude during the supercontinuum generation. The numerical study of the manifold broadening of the spatial and frequency spectra of the pulse during filamentation is very time-consuming. The calculating grids contain usually up to 2^{12} nodes for the temporal (t) and radial (r) coordinates and more that 2^{14} integration steps over the evolution variable z. Nevertheless, the attempts to study the filamentation of pulses produced by real high-power femtosecond lasers have failed.

Analysis of a change in the spatial scales of the light field in the beam cross section allows one to construct an efficient calculating scheme, which considerably expands the possibilities of numerical simulations. In the region near the beam axis, where a narrow intense filament is localised, small-scale structures appear in the complex amplitude of the light field, whereas the field intensity and phase remain slowly varying functions in the beam cross section. Such fields can be calculated by constructing a grid that is nonuniform over the radial coordinate. In the region near the beam axis, a small step of a few micrometres is used, which is necessary to reproduce the small-scale structure of the filament field. The radial step slowly increases with distance from the beam axis and achieves a few hundreds of micrometres at the beam periphery where the field varies slowly.

To construct a conservative nonuniform difference grid, it is convenient to pass to the variation formulation of the linear diffraction problem. The action functional $S[E, E^*]$ for the axially symmetric case has the form [35]

$$S[E, E^*] = \int_0^z \mathrm{d}z \int_0^\infty \left[\mathrm{i}k_0\left(E\,\frac{\partial E^*}{\partial z} - E^*\,\frac{\partial E}{\partial z}\right) - \frac{\partial E}{\partial r}\,\frac{\partial E^*}{\partial r}\right] r\,\mathrm{d}r. \qquad (10)$$

For $z = 0$, the function $E(r, z, t)$ satisfies equation (9). The stability condition for the functional $\delta S[E, E^*] = 0$ gives a linear equation for the diffraction of a restricted beam

$$2\mathrm{i}k_0\,\frac{\partial E}{\partial z} = \Delta_\perp E \qquad (11)$$

with the initial condition (9) for $z = 0$ and the boundary conditions

$$\lim_{r\to\infty} E = 0, \quad \left.\frac{\partial E}{\partial r}\right|_{r=0} = 0. \qquad (12)$$

Therefore, the complex amplitude $E(r, z, t)$, at which the functional $S[E, E^*]$ takes a stationary value, is a solution of the linear diffraction problem (11) with conditions (9) and (12).

Functional (10) can be represented on the grid $r \in [r_n, r_{n+1}]$ as a sum of integrals over its cells. Then, the functional can be written in the form

$$S_{\Delta z}[E, E^*] = \int_{z_s}^{z_{s+1}} \mathrm{d}z \times \sum_{n=0}^{N-1} \int_{r_n}^{r_{n+1}} \left[\mathrm{i}k_0\left(E\,\frac{\partial E^*}{\partial z} - E^*\,\frac{\partial E}{\partial z}\right) - \frac{\partial E}{\partial r}\,\frac{\partial E^*}{\partial r}\right] r\mathrm{d}r \qquad (13)$$

at one step $\Delta z = z_{s+1} - z_s$ of integration over z. At the step Δz, the field $E(r, z, t)$ inside a separate cell for $r \in [r_n, r_{n+1}]$ is approximated by a linear dependence over the radial (r) and evolution (z) variables:

$$E(r, z, t) = E_n^{(s)} + \frac{E_{n+1}^{(s)} - E_n^{(s)}}{r_{n+1} - r_n}(r - r_n) + \frac{E_n^{(s+1)} - E_n^{(s)}}{z_{s+1} - z_s}(z - z_s) + \frac{E_{n+1}^{(s+1)} - E_n^{(s+1)} - E_{n+1}^{(s)} + E_n^{(s)}}{(z_{s+1} - z_s)(r_{n+1} - r_n)}(r - r_n)(z - z_s), \qquad (14)$$

$$r \in [r_n, r_{n+1}],\ n = 0, 1, \ldots, N,$$

$$z \in [z_s, z_{s+1}],\ s = 0, 1, \ldots, S,\ E_n^{(s)} = E(r_n, z_s, t).$$

The parametric representation of the field (14) in grid cells allows us to calculate integrals in (13). The variation of the obtained expression over the node values $E_n^{(s)*}$ of the field yields a conservative finite difference scheme of the Cranck–Nickolson type, which is solved by the sweep method.

The technique for constructing nonuniform conservative grids over the radial variable makes it possible to create efficient numerical schemes for the multidimensional prob-

lems of nonlinear optics. This approach was considered in [35, 36] and was used in [12] to study the stationary self-focusing of a laser beam.

The step $\Delta r = r_{n+1} - r_n$ of the calculating grid over the radial variable in the problem of filamentation of a laser pulse was chosen so that it is not small and does not change in the region of size R_0 near the beam axis, where the light field of the pulse is small-scale, whereas outside this region ($r \geqslant R_0$) the step slowly increases according to the dependence

$$\frac{r_{n+1} - r_n}{r_n - r_{n-1}} = \varepsilon, \tag{15}$$

where the rise parameter is $\varepsilon \geqslant 1$. The step Δr, the size R_0 of the region near the beam axis and of the calculating aperture (A) for the entire grid, and the rise parameter are chosen in accordance with the physical parameters of a specific problem. For example, for the initial beam radius $a_0 = 3.5$ mm, the grid parameters are: $\Delta r = 1$ μm, $R_0 = 300$ μm, $A = 14$ mm, $\varepsilon = 1.0287$. The calculating grid contained 512 nodes over the radial variable and its step at the beam periphery achieved 400 μm. The accuracy of the reproduction of a light field in the beam cross section using this grid was not inferior than the accuracy obtained with the uniform grid with the step $\Delta r = 1$ μm containing 14 000 nodes.

The peak intensity and, hence, the nonlinear phase incursion at the integration step Δz increase infinitely, which can result in errors in the numerical analysis. To exclude such errors, the value of Δz was decreased, taking into account the conditions of the conservation of energy and Hamiltonian of the system [35], as well as a limited increment in the intensity and phase of the field at the integration step Δz. The initial integration step $\Delta z_0 = 0.01 k_0 a_0^2$ was decreased down to $0.01\Delta z_0$ during calculations.

5. Energy redistribution in a pulse

Numerical studies were performed for experimental conditions [7] where the output parameters of a femtosecond laser system were: $\lambda = 0.8$ μm, the pulse duration $\tau_0 = 140$ fs, the beam radius $a_0 = 3.5$ mm, the pulse energy $W = 10$ mJ, the peak power $P_{\max} = 38$ GW, and the initial intensity $I_0 \approx 10^{11}$ W cm^{-2}. The critical power $P_{\rm cr}$ of the self-focusing of a long pulse was assumed equal to 6 GW, as observed in experiments [7].

Fig. 4 shows the equal-intensity lines in the r, τ plane (where $\tau = t - z/v_{\rm gr}$ is the running time) for different distances z. At the scale chosen, the equal-intensity lines for the output pulse of the laser system represent concentric circles. The intensity increases at the filament onset ($z = 28$ m) for $\tau \geqslant 0$ in the temporal slice of the pulse which is located behind the slice with the peak intensity. Such a delay occurs due to the contribution of the inertial component of the cubic susceptibility which causes self-focusing. In the vicinity of the slice with $\tau \geqslant 0$, the equal-intensity lines are pulled to the axis and become more closely spaced, whereas their arrangement at the leading edge ($\tau/\tau_0 < -0.5$) does not change. The intensity of the central slices of the pulse increases up to 10^{13} W cm^{-2}, resulting in the generation of a laser plasma at the beam axis and defocusing of the subsequent slices of the pulse. For $z = 31$ m, the temporal slice, in which the intensity reaches a maximum equal to 6×10^{13} W cm^{-2}, shifts to the leading edge of the pulse ($\tau/\tau_0 < 0$). The intensity changes nonmonotonically in the radial direction at the pulse tail, suggesting the formation of a multi-ring structure. As the distance z increases up to 38 m, the intensity maximum shifts further to the leading edge of the pulse and remains invariable. The radius of the expanding intensity rings achieves the doubled radius of the initial beam.

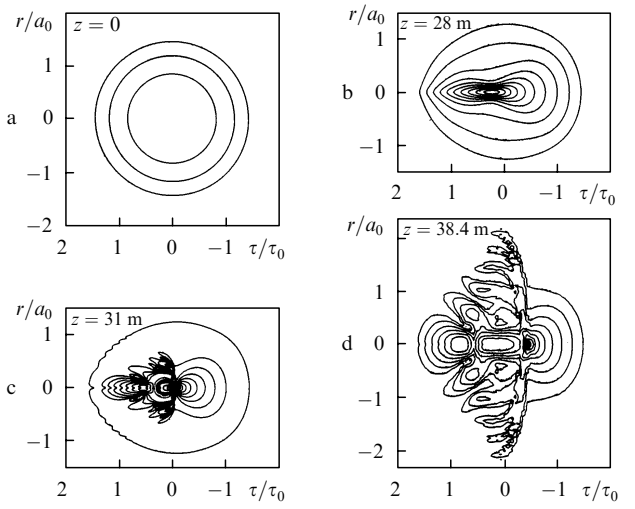

Figure 4. Equal-intensity lines $I(r, z, t)$ for different z for $\tau_0 = 140$ fs, $a_0 = 3.5$ mm, $I_0 \approx 10^{11}$ W cm^{-2}, and $W = 10$ mJ. The lines are shown for $I_n = 2^n I_0 0$, where $n = -3, -2, \ldots, +9$.

Defocusing in the laser plasma produced in a nonlinear focus gives rise to a component of the light field, which diverges from the beam axis. The superposition of this component and the background field results in the formation of a ring structure in the energy distribution in the beam cross section. In the numerical simulation, which reproduces the transformation of a real pulse, as in experiments, the fluence rings encompass a region whose transverse size greatly exceeds the filament diameter and is larger than the initial beam diameter (Fig. 1b).

The radiation power is redistributed in the beam cross section during self-focusing and formation of the ring structure. As an example, Fig. 5 shows the dependences of the radiation power on the distance in different regions of the beam cross section for one temporal slice of the pulse. We considered a circular region of radius 0.5 mm on the axis, in which the output energy is usually measured, and two ring regions: the central region, corresponding to the initial beam and having the inner and external radii of 0.5 and 3.5 mm, respectively, and the peripheral region with radii of 3.5 and 8.0 mm (see insert in Fig. 5). The initial power in the axial region was no more than 2 % of the total power, in the central region of about 60 %, and in the peripheral region of about 40 %.

During Kerr self-focusing, the low-intense background field propagates from the beam periphery to its axis, compensating for the energy in a moving focus forming a filament. At first ($z \leqslant 20$ m) the radiation field of the slice under study ($\tau = -20$ fs) is pulled from the peripheral region to the axial and central regions, where the radiation power slowly increases with distance. Directly in front of the

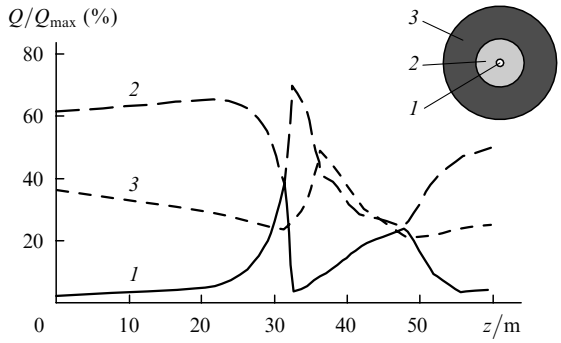

Figure 5. Dependences of the normalised power Q/Q_{max} on the distance z in different spatial regions of the temporal slice for $\tau = -20$ fs: in the axial region of radius 0.5 mm (*1*), in a ring with the internal and external radii of 0.5 and 3.5 mm, respectively (*2*), and in a ring with radii of 3.5 and 8 mm (*3*). The initial parameters of the radiation pulse are as in Fig. 4. The insert shows the positions of the regions in a plane perpendicular to the direction of the pulse propagation.

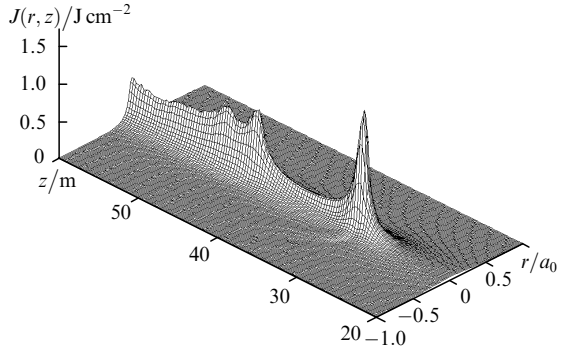

Figure 6. Distribution of the fluence $J(r,z)$ for the same initial parameters of the radiation pulse as in Fig. 4.

nonlinear focus for $z \approx 30$ m, the radiation power in the axial region (where the intensity has a maximum) rapidly increases due to its transfer from the central region, where it decreases. In the focus, the powers in the axial and peripheral regions are close to each other, each of them being ~ 40 %. The formation of the nonlinear focus on the axis does not affect the process of the power reduction in the peripheral region of the beam. A strong divergence of radiation in the self-induced laser plasma behind the nonlinear focus results in the formation of expanding rings, which transfer the radiation power over the beam cross section. In the axial region, radiation rapidly decreases because of rapid transfer to the central region and then to the peripheral region. Then ($z \leqslant 45$ m), some rings contract to the axis due to refocusing [7, 19], and the radiation power again transfers to the axial region. In this case, the external rings of the structure continue to expand, by transferring radiation power from the peripheral region of the pulse slice under study.

Our analysis showed that the transfer of radiation power over the beam cross section occurs in the region whose size exceeds considerably the filament size and the beam diameter at the laser output. At the same time, due to the combination of the dynamic processes of Kerr focusing of the leading edge of the pulse and defocusing of its tail in the laser plasma, the distribution of the fluence in the pulse measured in experiments very weakly changes with distance in a stable filament. Fig. 6 shows the dependence of the radial distribution $J(r)$ of the fluence in the pulse on the distance z. The maximum of $J(r)$ lies on the beam axis ($r = 0$), corresponding to the localisation of the radiation energy in the filament observed in experiments. At first, it changes nonmonotonically with distance z: drastically increases at $z = 30$ m, then decreases and again increases. Then, the radial distribution of the fluence is stabilised in the produced filament ($z > 40$ m). The nonmonotonic change in the filament energy at the initial stage, which is known as refocusing, was first observed in paper [7]. The filament energy is measured in experiments as the energy propagated during the pulse through a diaphragm of diameter 100–500 μm located on the beam axis. For the dependence presented in Fig. 6, the relative filament energy for a diaphragm of diameter 250 μm achieves the maximum equal to 12 % and is stabilised at the level 6 %–9 %, which is close to experimental data [7]. Note that the earlier attempts to obtain the quantitative agreement between numerical simulations of the energy characteristics of filaments and experimental data have failed.

6. Generation of a supercontinuum

The nonlinear self-modulation of the phase of the light field with a ring structure gives rise to the conical supercontinuum emission. The time gradient of the phase of the light field causes a very strong broadening of the frequency spectrum of the pulse, while the spatial gradient is responsible for the angular divergence of the short-wavelength branch of the spectrum [21]. The generation of a supercontinuum occurs not only in the vicinity of the filament but also in the ring structure embracing the filament. The region of the drastic spatial and temporal change in the radiation intensity and, hence, of the nonlinear phase incursion lies inside a circle whose radius is not smaller than the radius of the initial beam (Figs 4c, d). The numerical simulation of a broad range of the spatial scales of the field over the entire cross section of the pulse give a supercontinuum extending to the short-wavelength region to 0.4 μm, as was observed in experiments [9] (Fig. 2). Note that the spectral intensity of the short-wavelength components of the calculated spectrum is lower than the experimental intensity. This is explained by the fact that numerical simulations were performed for a pulse that had a longer duration and lower peak intensity than experimental pulses. According to [9], the efficiency of conversion of the fundamental radiation frequency to supercontinuum tails decreases with increasing pulse duration and decreasing its peak power. The propagation of a pulse under experimental conditions [9] is accompanied by the appearance of many filaments [33] whose formation cannot be calculated within the cylindrical symmetry used in this paper. At the same time, the limited computing resources do not allow the solution of equation (7) in the coordinates x, y, z, t.

The angular divergence of the spectral components of the visible region of a supercontinuum calculated numerically is close to the experimental data obtained in the wavelength region from 0.76 to 0.5 μm [7] (Fig. 3). For the divergence angle θ obtained in numerical simulations with an adequate reproduction of the spatial transformation

of the pulse field, the deviation from the experimental data does not exceed 20 % – 30 %.

7. Conclusions

In this paper, we have performed the numerical simulation of filamentation of a high-power femtosecond laser pulse in air taking into account the nonlinear-optical transformation of the light field of the pulse not only within a narrow axial region of energy localisation but also over its entire cross section. The numerical simulation was carried out using the efficient computing grid, which allows us to reproduce a broad range of spatial and temporal scales of the light field produced upon filamentation. We considered the filamentation of pulses whose parameters coincide with the parameters of pulses emitted by real high-power femtosecond lasers.

The characteristics of the filamentation process are obtained which are quantitatively close to the experimental data. The calculated distributions of the fluence in the beam cross section have a multiring structure, as in experiments. At the filament onset, its energy changes nonmonotonically with distance because of refocusing and then the energy is stabilised at a level of 6 % – 9 % of the total pulse energy. The supercontinuum in the visible region is extended to 0.4 μm. The divergence angle of conical emission in the visible region amounts to 0.1° at a wavelength of 0.5 μm.

It is shown that the localisation of energy in the filament, the dynamic stabilisation of its parameters, the formation of the multiring structure in the fluence distribution over the pulse cross section, the generation of a broadband supercontinuum, and conical emission observed in the visible region of the supercontinuum occur due to the nonlinear-optical transformation of the light pulse of the entire pulse in the region whose dimensions greatly exceed the filament diameter.

It is found that the radiation power is redistributed over the entire cross section of the temporal slices of the pulse during its filamentation. During self-focusing, a low-intense field for the peripheral region is contracted to the axis, compensating for the energy in the moving focus forming the filament. Aberration defocusing in a self-induced laser plasma results in the formation of the dynamic system of expanding rings, which rapidly transfer the radiation power for the axial region to the beam periphery. The contraction of the rings to the beam axis upon refocusing results in the returning of a part of the radiation power to the axial region.

Acknowledgements. This work was supported by the Russian Foundation for Basic Research (Grant No. 00-02-17497).

References

1. Corkum P.B., Rolland C., Srinivasan-Rao T. *Phys. Rev. Lett.*, **57**, 2268 (1986).
2. Wood W.M., Siders C.W., Downer M.C. *IEEE Trans. Plasma Sci.*, **21**, 20 (1993).
3. Belenov E.M., Nazarkin A.V., Prokopovich I.P. *Zh. Eksp. Teor. Fiz.*, **105**, 28 (1994).
4. Kandidov V.P., Kosareva O.G., Shlenov S.A. *Kvantovaya Elektron.*, **21**, 971 (1994) [*Quantum Electron.*, **24**, 905 (1994)].
5. Braun A., Korn G., Liu X., Du D., Squier J., Mourou G. *Opt. Lett.*, **20**, 73 (1995).
6. Nibbering E.T.J., Curley P.F., Grillon G., Prade B.S., Franco M.A., Salin F., Mysyrowicz A. *Opt. Lett.*, **21**, 62 (1996).
7. Brodeur A., Chien C.Y., Ilkov F.A., Chin S.L., Kosareva O.G., Kandidov V.P. *Opt. Lett.*, **22**, 304 (1997).
8. Kosareva O.G., Kandidov V.P., Brodeur A., Chien C.Y., Chin S.L. *Opt. Lett.*, **22**, 1332 (1997).
9. Kasparian J., Sauerbrey R., Mondelain D., Niedermeier S., Yu J., Wolf J.-P., Andre Y.-B., Franco M., Prade B., Tzortzakis S., Mysyrowicz A., Rodriguez M., Wille H., Woste L. *Opt. Lett.*, **25**, 1397 (2000).
10. Rairoux P., Schillinger H., Niedermeier S., Rodriguez M., Ronneberger F., Sauerbrey R., Stein B., Waite D., Wedekind C., Wille H., Woste L., Ziener C. *Appl. Phys. B*, **71**, 573 (2000).
11. Woste L., Wedekind C., Wille H., Rairoux P., Stein B., Nikolov S., Werner C., Niedermeier S., Ronneberger F., Schillinger H., Sauerbrey R. *Laser und Optoelektronik*, **29**, 51 (1997).
12. Lugovoi V.N., Prokhorov A.M. *Pis'ma Zh. Eksp. Teor. Fiz.*, **7**, 153 (1968).
13. Kosareva O.G., Kandidov V.P., Brodeur A., Chin S.L. *J. Nonlinear Opt. Phys. & Mater.*, **6**, 485 (1997).
14. Akozbek N., Bowden C.M., Talebpour A., Chin S.L. *Phys. Rev. E*, **61**, 4540 (2000).
15. Schwarz J., Diels J.-C. *Phys. Rev. A*, **65**, 013806 (2001).
16. Akhmanov S.A., Sukhorukov A.P., Khokhlov R.V. *Zh. Eksp. Teor. Fiz.*, **50**, 1537 (1966).
17. Vorob'ev V.V. *Izv. Vyssh. Uchebn. Zaved., Ser. Radiofiz.*, **13**, 1905 (1970).
18. Kandidov V.P., Kosareva O.G., Brider A., Chin S.L. *Opt. Atmos. Okean.*, **10**, 1539 (1997).
19. Mlejnek M., Wright E.M., Moloney J.V. *Opt. Lett.*, **23**, 382 (1998).
20. Chiron A., Lamouroux B., Lange R., Ripoche J.-F., Franko M., Prade B., Bonnaud G., Riazuelo G., Mysyrowicz A. *Europ. Phys. J. D*, **6**, 383 (1999).
21. Golubtsov I.S., Kandidov V.P., Kosareva O.G. *Opt. Atmos. Okean.*, **14**, 335 (2001).
22. Kandidov V.P., Kosareva O.G., Tamarov M.P., Broder A., Chin S.L. *Kvantovaya Elektron.*, **29**, 73 (1999) [*Quantum Electron.*, **29**, 355 (1999)].
23. Chin S.L., Talebpour A., Yang J., Petit S., Kandidov V.P., Kosareva O.G., Tamarov M.P. *Appl. Phys. B*, **74**, 67 (2002).
24. Kasparian J., Sauerbrey R., Chin S.L. *Appl. Phys. B*, **71**, 877 (2000).
25. Petit S., Liu W., Iwasaki A., Nadeau M.-C., Chin S.L., Kandidov V.P., Kosareva O.G., Andrianov K.Yu. *Opt. Commun.*, **210**, 329 (2002).
26. Chin S.L., Akozbek N., Proulx A., Petit S., Bowden C.M. *Opt. Commun.*, **188**, 181 (2001).
27. Perelomov A.M., Popov M.V., Terent'ev M.V. *Zh. Eksp. Teor. Fiz.*, **50**, 1393 (1966).
28. Talebpour A., Yang J., Chin S.L. *Opt. Commun.*, **163**, 29 (1999).
29. Akozbek N., Scalora M., Bowden C.M., Chin S.L. *Opt. Commun.*, **191**, 353 (2001).
30. Golubtsov I.S., Kosareva O.G. *Opt. Zh.*, **69** (7), 21 (2002).
31. Oleinikov P.A., Platonenko V.T. *Laser Phys.*, **3**, 618 (1993).
32. Nibbering E.T.J., Grillon G., Franco M.A., Prade B.S., Mysyrowicz A. *J. Opt. Soc. Am.*, **14**, 650 (1997).
33. Marburger J.H. *Prog. Quantum Electron.*, **4**, 35 (1975).
34. Raizer Yu.P. *Fizika gazovogo razryada* (Physics of a Gas Discharge) (Moscow: Nauka, 1992).
35. Chesnokov S.S., Egorov K.D., Kandidov V.P., Vysloukh V.A. *Intern. J. Num. Meth. Eng.*, **14**, 1581 (1979).
36. Dyshko A.L. *Zh. Vych. Matem. Fiz.*, **8**, 238 (1968).